3.2. Effects of microbubble concentration on spinal gene transfection

Fig. 2b shows the spinal luciferase activities one day after ultrasonication with 0, 20, and 50% MB. While the treatment with MB significantly increased the luciferase activities ($p<0.02$), the difference between 20 and 50% MB was not significant.

3.3. Time course of spinal gene expression

The spinal luciferase activities were analyzed at 1, 3, and 7 days after the intrathecal gene transfection using US and 50% MB (Fig. 2c). The luciferase activities significantly increased at 1 and 3 days post-transfection ($p<0.02$) without an intergroup difference, and returned to a level similar to that without US (at 1 day post-treatment) after 7 days.

3.4. Histological localization of the transfected gene expression

The immunohistochemical staining revealed that luciferase expression was mostly limited to the meningeal cells in the dorsal surface of the spinal cord (Fig. 3). The expressing regions were likely to have been the dura mater because Fig. 3b clearly shows a positive staining for cells in a membrane structure apart from the spinal parenchyma by the space of medullary fluid. As the dura mater consists of two cell types, meningeal cell and endothelial cell, the present data cannot strictly exclude the positive staining for the endothelial cells. However, the endothelial cells are shown to be very minor cellular component, so that frequent staining may indicate expression of the gene product mainly in the meningeal cells. There were no hemorrhage or inflammatory findings in the sections.

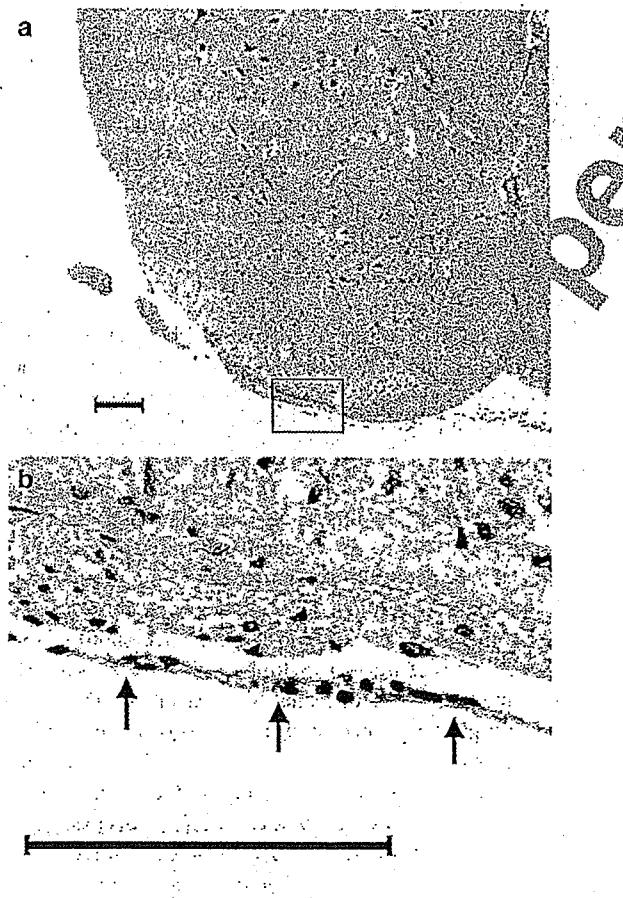

Fig. 3. Local gene expression in mouse spinal cord after intrathecal gene delivery using ultrasound and microbubbles. Expression of luciferase protein was mostly limited to the dorsal meningeal cells. (a) H&E staining in coronal sections of the lumber spinal cord. (b) Immunohistochemical localization of luciferase (arrows). Scale bar=100 μm.

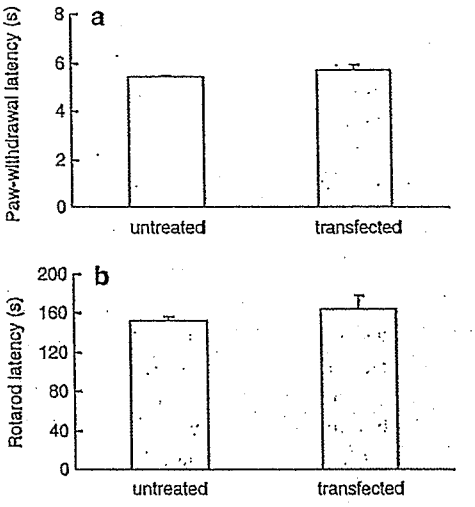

Fig. 4. Neurological evaluations of mice obtained 3 days after gene transfection using ultrasound and microbubbles (50%). (a) Paw-withdrawal latency following exposure to infra-red radiant heat. Three determinations each in the right and left hind paw were combined in each animal because the latency did not differ between the two sides. (b) Rotarod latency that represents the total time mice remained on the rotarod. Each mouse was tested with three trials. No significant difference was found compared to untreated mice in either determination. $n=4$ in each group. US: ultrasound; MB: microbubble (Optison).

3.5. Paw-withdrawal and rotarod latencies

Fig. 4 shows the averaged paw-withdrawal (Fig. 4a) and rotarod latencies (Fig. 4b) in untreated and transfected (DNA+50% MB+US) mice. Since the withdrawal latencies were not different between the right and left paw (data not shown), the data were combined in each animal. The determinations revealed no significant difference in the paw-withdrawal or rotarod latencies between the two groups, indicating that the present intervention did not affect the sensory and motor neurologic functions of the mice.

4. Discussion

The present study clearly demonstrated that percutaneous ultrasonication on an intrathecally administered mixture of plasmid-DNA and Optison facilitated the transfection of luciferase genes into the spinal meningeal cells in mice. No significant deficit was observed either in the sensory or motor neurologic functions after the procedures. In addition to the

general benefits of the combined use of ultrasound and microbubbles, our approach offers some advantages specific to spinal gene transfection. First, it requires only intrathecal needle access and percutaneous sonication that have been widely accepted in the clinical practice. Although a relatively short duration of gene expression (<7 days) was observed (Fig. 2c), the minimal invasiveness of the present surgical interventions would permit repetitive gene delivery into the spinal cord. Second, the intervertebral foramina and spaces would provide highly selective anatomical windows for ultrasound access while the vertebral bony structures would protect the spinal cord from possible excessive sonication. Although spotty gene expressions in the insonated regions would not be obvious in animals as small as the mice used in this study (Fig. 1), it can be expected that an ultrasound beam could reach the regions of the dorsal roots or the dorsal horns at targeted vertebral levels through the boneless apertures in large animals including human. This can be especially promising for transferring antinociceptive genes. Third, gene transfer into meningeal cells (Fig. 3) may be useful for topical delivery of bioactive substances into the CSF or adjacent spinal parenchyma while avoiding direct genetic modulation of parenchyma cells. Transgene-derived peptides such as growth factors, neuropeptides, or endogenous opioids that are secreted from meningeal cells would act in a paracrine manner on neurons and glias in the near vicinity, circumventing pharmacological problems related to the short half-life of the peptides or the need for high doses to achieve biological activity that could result in undesirable side effects.

Spinal gene therapy can be expected to be a promising approach to treat various spinal-related disorders. In previous animal studies, the delivery of therapeutic genes into the spinal nerve system has been mostly achieved using viral vectors [8]. However, because of the considerable disadvantages involved in using viral vectors, the development of alternative non-viral transgene techniques is needed. Cationic reagents such as cationic liposomes [17] have been developed for non-viral gene transfection. Achieving the efficient delivery of such molecules, however, to the spinal cord includes inherent difficulties. First, intrathecal injection induces diffusion of reagents into the cerebral spinal fluid (CSF), resulting in lack of target specificity. Second, since the CSF continuously circulates and replaces, a constant concentration of reagents for necessary transfection to a specific site would not be achieved. Ultrasound gene therapy is an alternative non-viral approach [18]. The insufficient transfection efficiency of simple ultrasonication can be improved by the combined use of echo-contrast microbubbles [11]. The use of ultrasound with microbubbles, which enables non-invasive, tissue-specific gene delivery, has received much interest and enhanced gene transfer has been reported in various animal tissues *in vivo* including heart [19], peripheral arteries [20], skeletal muscles [21], and brain [22]. Very recently, Shimamura et al. reported successful gene transfer into the rat spinal cord using ultrasound and microbubbles [23]. The authors intrathecally injected naked luciferase DNA with Optison through the 4/5th lumbar intervertebral space and applied sonication directly on the thoracic dural sac by removing the dorsal part of the 9–10th thoracic vertebra, which resulted in the enhanced expression of luciferase in the meningeal cells in the insonated region. In contrast, we accomplished transgene expression in the meningeal cells by intrathecal injection of luciferase DNA with Optison through the lower lumbar intervertebral space, as in their study, but then employed simple transcutaneous insonation at the same lumbar region without surgical exposure of the dura. The lower invasiveness in our methodology would seem to be more clinically useful. Interestingly, the duration of transgene expression was consistently as short as a week in both studies. Although Shimamura et al. described that the short expression of transgene by single transfection would be acceptable to treat acute spinal cord trauma [23], the repeated applicability due to the lower invasiveness in the present study could enable treatments for chronic ailments. In fact, we have recently shown that successive gene expression was obtained by repeat transfection using the present ultrasound–microbubble technique [24]. Nonetheless, since gene expression for longer than 3 weeks was previously achieved by spinal electroporation via an intrathecal electrode catheter in rat meningeal cells [25,26], the present ultrasound–microbubble approach has the potential for methodological improvement to prolong the duration of transgene expression by optimizing acoustic parameters such as intensity, duty ratio, frequency, and spatial pressure distribution [12] and changing the membrane properties of microbubbles [27].

The present acoustic parameters were relatively consistent with those reported in previous studies in which ultrasound and Optison were safely used for transferring genes into nervous tissues [22,23]. Consistent with those studies, we did not find macroscopic injuries in the skin or muscles, microscopic damage in the spinal cord, or significant deficits in the spinal neurological functions. In addition, the present neurological tolerance may be alternatively explained by a characteristic of our approach, namely that the intact vertebral bony structures surrounding the intervertebral apertures limited excessive sonication of the spinal cord. Nonetheless, further optimization of the ultrasound parameters will improve the safeness of sonication on nervous tissues. The physical conditions of the microbubbles used in this study are additional issues to be discussed. First, although we evaluated only the usefulness of Optison, the possible utility and safety of microbubbles other than Optison (e.g. lipid microbubbles) for intrathecal gene transfer remains to be explored. Second, we should note that Optison at a concentration as high as 50% was used in most series of the present experiments. The reasons for this were that a trend of higher transfection efficacy was observed in the 50% group (but ns vs. 20% groups, Fig. 2b) and that no apparent neurological damage was observed in the transfected mice (Fig. 4). However, earlier studies [22,23] successfully used Optison at concentrations of 20–25% for intrathecal gene delivery in rats. It seems reasonable that intrathecal microbubbles at lower concentrations would induce fewer adverse effects while enabling an increase in the relative content of plasmid DNA in a limited volume of mixture. Therefore, it is possible that the concentration of microbubbles for intrathecal injection could be further optimized. The authors finally note

that the functional expressions of genes transfected into the spinal nerve system have not yet been examined. Further efforts using genes that are encoded with neurobioactive peptides are clearly needed to investigate the clinical usefulness of the present ultrasound–microbubble approach.

In conclusion, we demonstrated that simple percutaneous ultrasonication on intrathecally administered plasmid DNA and echo-contrast microbubbles enhanced the gene transfer into spinal meningeal cells in mice. The present approach can provide some advantages specific to spinal gene therapy including minimal invasiveness, regional targetability, and possible paracrine delivery of therapeutic molecules to the spinal nerve system. Studies including functional assessments of therapeutic gene transfer as well as the application of the techniques in larger animals will further clarify the feasibility of the present ultrasound–microbubble method in spinal gene therapy.

References

[1] J.C. Glorioso, D.J. Fink, Herpes vector-mediated gene transfer in treatment of diseases of the nervous system, Annu. Rev. Microbiol. 58 (1) (2004) 253–271.

[2] S.P. Wilson, Gene-based therapy for treatment of chronic pain, Semin. Pain Med. 1 (4) (2003) 220–226.

[3] F. Facchiano, E. Fernandez, S. Mancarella, G. Maira, M. Miscusi, D. D'Arcangelo, G. Cimino-Reale, M.L. Falchetti, M.C. Capogrossi, R. Pallini, Promotion of regeneration of corticospinal tract axons in rats with recombinant vascular endothelial growth factor alone and combined with adenovirus coding for this factor, J. Neurosurg. 97 (1) (2002) 161–168.

[4] M. Koda, M. Hashimoto, M. Murakami, K. Yoshinaga, O. Ikeda, M. Yamazaki, S. Koshizuka, T. Kamada, H. Moriya, H. Shirasawa, S. Sakao, H. Ino, Adenovirus vector-mediated in vivo gene transfer of brain-derived neurotrophic factor (BDNF) promotes rubrospinal axonal regeneration and functional recovery after complete transection of the adult rat spinal cord, J. Neurotrauma 21 (3) (2004) 329–337.

[5] X.Q. Tang, Y. Wang, Z.H. Huang, J.S. Han, Y. Wan, Adenovirus-mediated delivery of GDNF ameliorates corticospinal neuronal atrophy and motor function deficits in rats with spinal cord injury, NeuroReport 15 (3) (2004) 425–429.

[6] S.P. Wilson, D.C. Yeomans, M.A. Bender, Y. Lu, W.F. Goins, J.C. Glorioso, Antihyperalgesic effects of infection with a preproenkephalin-encoding herpes virus, Proc. Natl. Acad. Sci. U. S. A. 96 (6) (1999) 3211–3216.

[7] A.A. Finegold, A.J. Mannes, M.J. Iadarola, A paracrine paradigm for in vivo gene therapy in the central nervous system: treatment of chronic pain, Hum. Gene Ther. 10 (7) (1999) 1251–1257.

[8] M. Pohl, J. Braz, Gene therapy of pain: emerging strategies and future directions, Eur. J. Pharmacol. 429 (1–3) (2001) 39–48.

[9] M. Mata, J. Glorioso, D.J. Fink, Development of HSV-mediated gene transfer for the treatment of chronic pain, Exp. Neurol. 184 (Suppl. 1) (2003) S25–S29.

[10] P.A. Dijkmans, L.J.M. Juffermans, R.J.P. Musters, A. van Wamel, F.J. ten Cate, W. van Gilst, C.A. Visser, N. de Jong, O. Kamp, Microbubbles and ultrasound: from diagnosis to therapy, Eur. J. Echocardiog. 5 (4) (2004) 245–256.

[11] R. Bekeredjian, P.A. Grayburn, R.V. Shohet, Use of ultrasound contrast agents for gene or drug delivery in cardiovascular medicine, J. Am. Coll. Cardiol. 45 (3) (2005) 329–335.

[12] T. Kodama, Y. Tomita, K. Koshiyama, M.J.K. Blomley, Transfection effect of microbubbles on cells in superposed ultrasound waves and behavior of cavitation bubble, Ultrasound Med. Biol. 32 (6) (2006) 905–914.

[13] J.L. Hylden, G.L. Wilcox, Intrathecal morphine in mice: a new technique, Eur. J. Pharmacol. 67 (2–3) (1980) 313–316.

[14] B.W. Rice, M.D. Cable, M.B. Nelson, In vivo imaging of light-emitting probes, J. Biomed. Opt. 6 (4) (2001) 432–440.

[15] K.M. Hargreaves, R. Dubner, F. Brown, C. Flores, J. Joris, A new and sensitive method for measuring thermal nociception in cutaneous hyperalgesia, Pain 32 (1) (1988) 77–88.

[16] J.D. Hommel, R.M. Sears, D. Georgescu, D.L. Simmons, R.J. DiLeone, Local gene knockdown in the brain using viral-mediated RNA interference, Nat. Med. 9 (12) (2003) 1539–1544.

[17] C.R. Dass, P.F. Choong, Selective gene delivery for cancer therapy using cationic liposomes: in vivo proof of applicability, J. Control. Release 113 (2) (2006) 155–163.

[18] C.M. Newman, A. Lawrie, A.F. Brisken, D.C. Cumberland, Ultrasound gene therapy: on the road from concept to reality, Echocardiography 18 (4) (2001) 339–347.

[19] R. Bekeredjian, S. Chen, P.A. Frenkel, P.A. Grayburn, R.V. Shohet, Ultrasound-targeted microbubble destruction can repeatedly direct highly specific plasmid expression to the heart, Circulation 108 (8) (2003) 1022–1026.

[20] Y. Taniyama, K. Tachibana, K. Hiraoka, T. Namba, K. Yamasaki, N. Hashiya, M. Aoki, T. Ogihara, K. Yasufumi, R. Morishita, Local delivery of plasmid DNA into rat carotid artery using ultrasound, Circulation 105 (10) (2002) 1233–1239.

[21] Y. Taniyama, K. Tachibana, K. Hiraoka, M. Aoki, S. Yamamoto, K. Matsumoto, T. Nakamura, T. Ogihara, Y. Kaneda, R. Morishita, Development of safe and efficient novel nonviral gene transfer using ultrasound: enhancement of transfection efficiency of naked plasmid DNA in skeletal muscle, Gene Ther. 9 (6) (2002) 372–380.

[22] M. Shimamura, N. Sato, Y. Taniyama, M. Endo, H. Kurinami, M. Aoki, T. Ogihara, Y. Kaneda, R. Morishita, Development of efficient plasmid DNA transfer into adult rat central nervous system using microbubble-enhanced ultrasound, Gene Ther. 11 (20) (2004) 1532–1539.

[23] M. Shimamura, N. Sato, Y. Taniyama, H. Kurinami, H. Tanaka, T. Takami, M. Ogihara, Y. Tohyama, R. Morishita, Gene transfer into adult rat spinal cord using naked DNA and ultrasound microbubbles, J. Gene Med. 7 (11) (2005) 1468–1474.

[24] A. Aoi, K. Konno, S. Fumiaki, S. Mori, G. Vassaux, T. Kodama, HSV-tk/GCV cytotoxic gene therapy using ultrasound and nanobubbles, Ultrasound Med. Biol. 32 (5S) (2006) 280.

[25] C.R. Lin, M.H. Tai, J.T. Cheng, A.K. Chou, J.J. Wang, P.H. Tan, M. Marsala, L.C. Yang, Electroporation for direct spinal gene transfer in rats, Neurosci. Lett. 317 (1) (2002) 1–4.

[26] T.H. Lee, L.C. Yang, A.K. Chou, P.C. Wu, C.R. Lin, C.H. Wang, J.T. Chen, C.S. Tang, In vivo electroporation of proopiomelanocortin induces analgesia in a formalin-injection pain model in rats, Pain 104 (1–2) (2003) 159–167.

[27] J.R. Lindner, Microbubbles in medical imaging: current applications and future directions, Nat. Rev. Drug Discov. 3 (6) (2004) 527–532.

Minimally Invasive Therapy. 2006; 15:4; 226–229

Taylor & Francis
Taylor & Francis Group

ORIGINAL ARTICLE

A non-invasive tissue-specific molecular delivery method of cancer gene therapy

TETSUYA KODAMA[1], ATSUKO AOI[1], GEORGES VASSAUX[2], SHIRO MORI[3], HIDEHIRO MORIKAWA[3], KENI-CHIRO KOSHIYAMA[4], TAKERU YANO[4], SHIGEO FUJIKAWA[4] & YUKIO TOMITA[5]

[1]*Tohoku University Biomedical Engineering Research Organization, Sendai, Japan,* [2]*Cancer Research UK Clinical Centre at Barts and The London, Barts and The London School of Medicine and Dentristy, John Vane Science Centre, London, United Kingdom,* [3]*Tohoku University Hospital, Sendai, Japan,* [4]*Graduate School of Engineering, Hokkaido University, Sapporo, Japan, and* [5]*Faculty of Education, Hokkaido University of Education, Hakodate, Japan*

Abstract

A Japanese word, *monozukuri* (literally translated "making things") is the philosophy of first having the idea and then the faith in the technical expertise and experience to accomplish the result. We believe that the concept of engineering is *monozukuri*. Through the process of *monozukuri*, engineered natural science based on mathematics and physics has been developed. Medicine is the field of study which has been developed for maintaining daily healthy life with diagnosis, treatment, examination, and protection. Biomedical engineering is the interdisciplinary study of engineering and medicine, and should be developed based on *monozukuri*. In this particular research, we have developed a physical molecular delivery method for cancer gene therapy using nano/microbubbles and ultrasound. First, the behavior of cavitation bubbles and subsequent shock wave phenomena involved in the mechanism of molecular delivery were analyzed, combining theory and computer simulation. In a second step, the methodology was optimized *in vitro* and *in vivo*. Finally, the therapeutic potential of the method in pre-clinical models was evaluated using transgenes relevant to cancer gene therapy instead of reporter genes, and whole body, non-invasive imaging using single photon emission computed tomography (SPECT/CT) was used to evaluate the selectivity of gene delivery *in vivo*.

Key words: *Cavitation bubble, ultrasound, shock wave, imaging, molecular dynamics simulation*

Introduction

Non-invasive, tissue-specific molecular delivery is crucial for the efficiency and reduced side effects of a wide range of treatments. This is particularly the case in gene therapy applications. Nano/microbubbles (NMB), which are encapsulated gas bubbles with a diameter $<10\mu m$, have been developed with the aim of optimizing vascular imaging (1). Recently, a physical method that combines NMB with ultrasound (US) has been regarded as one of the few methods capable of delivering genes into target sites non-invasively. Conceptually, gene vectors mixed with NMB are injected either locally or systematically and targeted gene transfer is achieved by selective insonation of a defined area. Applied to cancer gene therapy, this method could efficiently target cancer, and may be more efficient than immune gene therapy, as patients are often immunocompromised. In addition, NMB can be used as a targeted marker of molecular imaging to detect angiogenesis in cancer, inflammation, and thrombus. This method is not toxic and non-immunogenic. However, several essential aspects remain unexplored. First, cavitation bubbles are believed to be a major mediator for molecular delivery, however, the relation between wave characteristics and subsequent generation and collapse of cavitation bubbles has not been elucidated, and therefore gene transfer has not been optimized. In addition, molecular delivery and subsequent gene expression have not been quantified *in vivo*.

Correspondence: T. Kodama, Biomedical Engineering Research Organization, Tohoku University, 2-1 Seiryo-machi, Aoba-ku, Sendai 980-8575, Japan. Fax: +81-22-717-7583. E-mail: kodama@tubero.tohoku.ac.jp

ISSN 1364-5706 print/ISSN 1365-2931 online
DOI: 10.1080/13645700600836059

In our research project, we conducted three main studies aimed at developing translational research in combination with the NMB and US (NMB-US) method (Figure 1). First, we optimized these ultrasound and cavitation parameters *in vitro* and *in vivo*, and elucidated the mechanism of molecular delivery with theoretical and computer analysis. Second, transgenes relevant to cancer gene therapy were delivered instead of a reporter gene to evaluate the therapeutic potential of the approach in pre-clinical models. Third, in addition to more classical immunohistochemical analysis, whole body, non-invasive imaging using single photon emission computed tomography (SPECT/CT) was used to evaluate the selectivity of gene delivery *in vivo*. This will be performed in pre-clinical rodent models and may be applied to patients at a later stage, as SPECT/CT imaging is scalable to humans.

Mechanism of molecular delivery with theoretical and computer analysis

In previous experiments it was found that NMB were completely destroyed at intensities $>0.5 W/cm^2$, resulting in the generation of nanobubbles. We hypothesize that these bubbles can behave as cavitation bubbles (Figure 2). Cavitation bubbles generate impulsive pressures such as liquid jet impact and shock wave. Liquid jet is generated due to non-symmetric collapse of a cavitation bubble and its direction and intensity depends on the dynamic properties of its surrounding boundaries. In general, liquid jets would not be generated near materials with high compliance (2); therefore, cavitation bubbles would not produce liquid jet near tissue. Shock waves are produced at the generation and rebound of cavitation bubbles, are attenuated as approximately $1/r$ (r: radial distance from the center of each bubble) while they are propagated. Shock

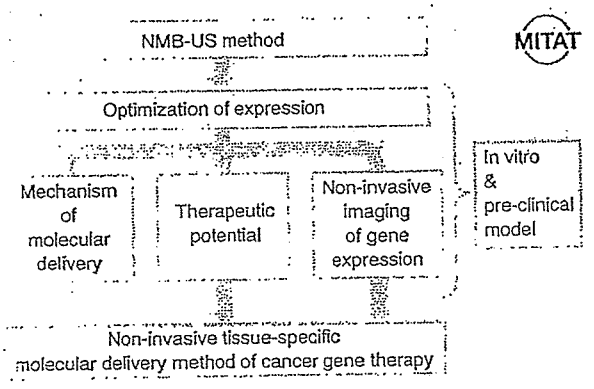

Figure 1. Projects aimed at developing translational research. NMB: nano/microbubbles, US: ultrasound.

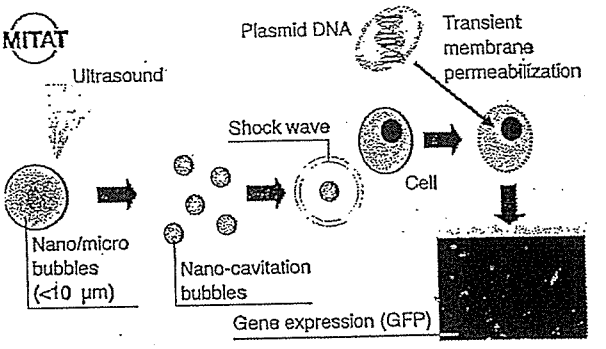

Figure 2. Mechanism of molecular delivery into cells using ultrasound and nano/microbubbles.

waves are nonlinear and finite-amplitude waves, and the flow induced by the shock waves can not be ignored. The displacement of liquid induced behind shock wave may have an effect on bio-material including cells. This movement of liquid may be related to the change in membrane permeability. Kodama et al. (3) reported that the impulse (defined as the integral of pressure with duration) of the shock wave might be an important factor governing the temporary permeability increase necessary for delivering macromolecules into cells.

To investigate the interaction of shock wave with cell membrane, we conducted molecular dynamics (MD) simulation (4). A cell membrane was designed as a 32 dipalmitoylphosphatidylcholine (DPPC) lipids bilayer, placed between two 1200 water molecules layers in the rectangular calculation box. The shock impulse per unit area I is defined as

$$I = \int_0^{t_+} p(t)\, dt, \qquad (1)$$

where t is the time, $p(t)$ the pressure near the cells in water, and t_+ the positive phase duration of a half cycle of the shock wave (3). In the MD simulation we observed that structural changes of the bilayer were induced by the impulse, followed by water molecule penetration into the hydrophobic region of the bilayer. In addition, we investigated the process of spontaneous water pore formation in the phospholipid bilayer, which is expected to occur after the water molecules penetration (5). Furthermore, we discussed the possibility of the uptake of 5 fluorouracil (5FU) into the bilayer in the presence of shock waves, which has been used in cancer therapy.

Stokes radius is the effective radius of a molecule that depends on the molecular weight and molecular configuration and has been used as a determination of transport through matrices (6). Stokes radius of the plasmid DNA was estimated to be 13 nm(2) if its length is 10kb, which is larger than water radius

(≈0.01nm) by a factor of 1300. The uptake of endogenous molecules depends not only on the impulse value, but also on the molecular weight (3,7) and the impulse times (8). The molecular weight of water is different from that of plasmid DNA and the mechanism of exogenous molecules incorporated into cells is a complex phenomenon. However, the present simulation will give valuable information on the mechanism of molecular delivery on the molecular level.

Therapeutic potential of the approach in pre-clinical models

Suicide gene therapy of cancer essentially requires efficient gene delivery and highly selective gene expression. One suicide gene therapy is to transfer cDNA of the herpes simplex virus thymidine kinase (HSV*tk*) gene into tumor cells, which sensitizes the cells to the normally non-toxic antiviral drug, ganciclovir (GCV) (9). The activity of antitumor effect results from HSV*tk* expressing tumor cells activating GCV to its cytotoxic triphosphate derivative. This derivative, when incorporated into replicating DNA, interferes with DNA chain elongation and results in cell death (10).

In the project we demonstrated the therapeutic potential of the NMB-US method of cancer gene therapy using HSV*tk*/GCV (11). We transduced HSV*tk* gene into five cell lines (A549, MCF7, EMT6, colon 26 and 293T cells) using albumin or lipid bubbles (10% v/v) under the optimized US conditions (frequency: 945kHz, duty ratio:50%, pressure: 0.96MPa). The mRNA of HSV*tk* expression was detected by real time PCR at 24h after gene transfer. The anti-cancer effects of GCV treatment were evaluated using MTT assay four days after gene transfer. Significant cytotoxity was obtained only in treated cells which expressed the mRNA of HSV*tk*, compared to untreated cells. These results suggest that GCV phosphorylated with HSV*tk* would induce specific cytotoxity to transfected cancer cells. Next, we tested this system *in vivo* and demonstrated that NMB-US mediated HSV*tk* gene transfer could result in a therapeutic effect in a mouse model of colorectal cancer. However, these studies are required to evaluate the full potential of this methodology.

Non-invasive imaging of gene expression

In gene therapy, non-invasive imaging of gene profile expressed in patients after gene transfer and effective treatment are required. In the third project, we investigated noninvasive imaging of gene expression using SPECT/CT, delivered with the NMB-US method. We showed that the NMB-US method could deliver of the sodium iodide symporter (NIS) gene *in vitro* and we are currently repeating the experiment *in vivo* with the aim to visualize and quantify gene expression measured by uptake of iodide *in vivo*.

Conclusions

Currently, this methodology is being developed and its full potential *in vivo* remains to be established. However, pilot studies have demonstrated the feasibility of gene transfer *in vivo* using the methodology and we expect that practical application will be developed. Therefore, by developing this new methodology from the design to the therapeutic applications, this project follows the general concepts of *monozukuri*.

Acknowledgments

We have collaborated with many other researches on the present project. Masao Ono, Yuji Owada, Graduate School of Medicine, Tohoku University, Masahiko Takahashi, Mirei Chiba, Graduate School of Dentistry, Tohoku University, Fumiaki Shinohara, Tohoku University Hospital, Masatoshi Itoh, Cyclotron and Radioisotope Center Tohoku University, Toshiyuki Hayase, Yasuaki Kohama, Institute of Fluid Science, Tohoku University, Manabu Fukumoto, Institute of Development, Aging and Cancer, Tohoku University, Yasuhiro Matsumura, National Cancer Center, Japan, Fumiaki Takahashi, Polytechnic College Miyagi, Apostolos Doukas, Michael Hamblin, Harvard Medical School, Massachusetts General Hospital.

This study was supported by grants from Special Coordination Funds for Promoting Science and Technology (MEXT), Grant-in-Aid for Scientific Research on Priority Area, MEXT (17012002, 18014002), Grant-in-Aid for Exploratory Research (18450140), Grant-in-Aid for Specially Promoted Research (B), JSPS (17300168), and Grant for Research on Advanced Medical Technology from the Ministry of Health, Welfare and Labour, Japan (H17-nano-006).

References

1. Lindner JR. Microbubbles in medical imaging: current applications and future directions. Nat Rev Drug Discov. 2004;3:527–32.
2. Kodama T, Tomita Y. Cavitation bubble behavior and bubble-shock wave interaction near a gelatin surface as a

study of in vivo bubble dynamics. Appl. Phys. B-Lasers. 2000;70:139–49.
3. Kodama T, Hamblin MR, Doukas AG. Cytoplasmic molecular delivery with shock waves: importance of impulse. Biophys J. 2000;79:1821–32.
4. Koshiyama K, Kodama T, Yano T, Fujikawa S. Molecular dynamic simulation of cell permeabilization induced by shock wave impulse. In: Ikohagi T, editor. Fourth International Symposium on Advanced Fluid Information and the First International Symposium on Transdisciplinary Fluid Integration. 2004; Sendai; 2004. p. 36–37.
5. Koshiyama K, Kodama T, Yano T, Fujikawa S. Molecular dynamics simulation of water pore formation in lipid bilayer induced by shock waves. In: The 5th International Symposium on Therapeutic Ultrasound. 2005; Boston, MA, USA; 2005. p. 98.
6. Bohrer MP, Deen WM, Robertson CR, Troy JL, Brenner BM. Influence of molecular configuration on the passage of macromolecules across the glomerular capillary wall. J Gen Physiol. 1979;74:583–93.
7. Gambihler S, Delius M, Ellwart JW. Permeabilization of the plasma membrane of L1210 mouse leukemia cells using lithotripter shock waves. J Membr Biol. 1994;141:267–75.
8. Kodama T, Doukas AG, Hamblin MR. Shock wave-mediated molecular delivery into cells. Biochim Biophys Acta. 2002;1542:186–94.
9. Moolten FL. Tumor chemosensitivity conferred by inserted herpes thymidine kinase genes: paradigm for a prospective cancer control strategy. Cancer Res. 1986;46:5276–81.
10. Chen SH, Chen XH, Wang Y, Kosai K, et al. Combination gene therapy for liver metastasis of colon carcinoma in vivo. Proc Natl Acad Sci U S A. 1995;92:2577–81.
11. Suzuki M, Shinohara F, Aoi A, Sato Y, et al. Application of nanobubbles for HSV*tk*/GCV cytotoxic gene therapy using ultrasound. In: ECCO 13-the European Cancer Conference; 2005; Paris, France; 2005. p. 57.

Biophysical Journal Volume 91 September 2006 2198–2205

Structural Change in Lipid Bilayers and Water Penetration Induced by Shock Waves: Molecular Dynamics Simulations

Kenichiro Koshiyama,* Tetsuya Kodama,† Takeru Yano,* and Shigeo Fujikawa*
*Division of Mechanical and Space Engineering, Hokkaido University, Sapporo, Japan; and †Biomedical Engineering Research Organization, Tohoku University, Sendai, Japan

ABSTRACT The structural change of a phospholipid bilayer in water under the action of a shock wave is numerically studied with unsteady nonequilibrium molecular dynamics simulations. The action of shock waves is modeled by the momentum change of water molecules, and thereby we demonstrate that the resulting collapse and rebound of the bilayer are followed by the penetration of water molecules into the hydrophobic region of the bilayer. The high-speed phenomenon that occurs during the collapse and rebound of the bilayer is analyzed in detail, particularly focusing on the change of bilayer thickness, the acyl chain bend angles, the lateral fluidity of lipid molecules, and the penetration rate of water molecules. The result shows that the high-speed phenomenon can be divided into two stages: in the first stage the thickness of bilayer and the order parameter are rapidly reduced, and then in the second stage they are recovered relatively slowly. It is in the second stage that water molecules are steadily introduced into the hydrophobic region. The penetration of water molecules is enhanced by the shock wave impulse and this qualitatively agrees with a recent experimental result.

INTRODUCTION

A cell permeabilization technique with shock waves is capable of introducing macromolecules and small polar molecules into the cytoplasm (1–7). This technique is definitely suitable for applications in gene therapy and anticancer drug delivery since shock waves can be focused into specific target sites of patients' bodies noninvasively. The primary concern in recent studies has been the efficiency of macromolecule delivery. Kodama et al. (6) have experimentally demonstrated that the permeability of cell membrane can be enhanced by the increase of the shock wave impulse defined as the time integral of pressure over the shock-pulse duration, irrespective of the peak pressure of the shock wave. The mechanism of the increase in permeability, however, remains unknown and the lack of the knowledge of the phenomenon still prevents the development of the applications mentioned above. Clearly, the microscopic information about the molecular transport across the membrane is required and it will be obtained by molecular dynamics (MD) simulations. In this study, we carry out unsteady nonequilibrium MD simulations of lipid bilayers of cell membranes subjected to the action of shock impulses. We thereby clarify the fundamental and important characteristics of the dynamical process of structural change in lipid bilayers and water penetration into the hydrophobic region of the bilayer.

The biological cell membranes are, as well known, composed of phospholipids, proteins, and carbohydrates, and models describing its structure continue to be revised and refined, beginning from the fluid mosaic model (8) to the lipid rafts microdomain models (9,10). Although the cell membranes in general have such complex structures, the fundamental and common element is the phospholipid bilayer. The method of MD simulations for cell membranes has been developed for the lipid bilayer accordingly. There are a number of important contributions about the numerical methodology, such as the force field (11), the charges of polar molecules (12), the effect of choice of ensembles (13), the treatment of the electrostatic interactions (14), and so on. On the basis of these contributions, works on the molecular transport across the bilayer are being published (15–18). The simulations of pore formation in lipid bilayer have also been performed recently (19–22).

However, we emphasize that much effort has been devoted to the research of an almost static configuration or slow translocation of lipid molecules. Dynamical processes of cell membranes under the action of shock waves have not been investigated with MD simulations so far, to our knowledge. The shock wave is a high pressure wave with a steep wave front that propagates at a supersonic speed, and it passes the cell membrane within a very short time of the order of picoseconds. Therefore, understanding a high-speed phenomenon induced by the interaction of shock waves with cell membranes should be indispensable to the advance of the gene/drug delivery technique with shock waves. We address this challenging problem in this work using unsteady nonequilibrium MD simulations.

METHODS

As mentioned in the Introduction, the interaction of shock waves with cell membranes is a high-speed phenomenon completed in a very short time because the thickness of the membrane is of the order of nanometers and the shock propagation speed is supersonic. Such high-speed phenomena have never been studied in the field of biomolecular dynamics, to our knowledge. Neither the simulation methods nor the analysis tools have been established.

Submitted January 18, 2006, and accepted for publication June 13, 2006.

Address reprint requests to Shigeo Fujikawa, E-mail: fujikawa@eng.hokudai.ac.jp.

0006-3495/06/09/2198/08 $2.00

doi: 10.1529/biophysj.105.077677

We therefore have to construct a new method for modeling of shock waves and new analysis tools. To avoid unexpected difficulties arising from newly introduced techniques, however, we make the most of existing methodology established in the equilibrium simulations with great care.

Lipid bilayer/water system

The simulations here have first been performed with a small bilayer/water system consisting of 32 dipalmitoylphosphatidylcholine (DPPC) lipids and 4800 water molecules in a rectangular simulation box. Thereafter, we have validated the results by conducting further simulations with a larger system of 128 lipids and 19,200 water molecules. This section explains the simulation method of the equilibrium bilayer/water system, which was utilized for an initial condition of shock wave simulation described in subsequent sections.

The refined united atom force field (23) with AMBER99 force field (24) was applied to the DPPC lipids. The atomic charges calculated by Chiu et al. (12) were used for DPPC, and they are illustrated in Fig. 1 with the molecular structure and AMBER atom types. The simulation procedure was substantially the same as an already established one (23). For water, the simple point charge model (25) was used. Lennard-Jones interactions were cut off at 1.0 nm, and long-range electrostatic interactions were handled by means of the particle mesh Ewald method (26) with Ewald coefficient 0.275.

The initial configuration of the bilayer/water system for shock wave simulation was prepared in an equilibration simulation (*NPT* computation), where the temperature and pressure were controlled using the weak coupling algorithm (27) with $\tau_T = 0.5$ ps, $T = 323$ K, $\tau_p = 1.0$ ps, and $p = 101.3$ kPa. The equations of motion of molecules were integrated employing the leap frog method with time step $\tau = 2.0$ fs, and the three-dimensional periodic boundary conditions were applied. After an ~8-ns run of equilibration simulation with the SHAKE algorithm (28), we obtained an equilibrated bilayer/water system of volume $7.18 \times 5.99 \times 17.51$ nm in the case of the larger system, where the linear dimension of the simulation box in the z direction normal to the bilayer plane (the xy plane) is 17.51 nm. The volume of the smaller system was $3.77 \times 2.72 \times 18.32$ nm.

Here, we remark that our bilayer/water system included a large water layer of thickness ~14 nm, whereas the thickness of the bilayer was ~4 nm. This is because this simulation of shock waves required a large number of water molecules, as explained below. Such a large water layer has also been used by Marrink et al. in an MD simulation of lipid adhesion (29).

Because we are interested in the dynamical process of structural change in bilayer resulting from shock wave irradiation, it may be better to remove the constraint of molecular bond lengths based on the SHAKE algorithm. We therefore continued the equilibrium simulation of the bilayer/water system without using SHAKE and confirmed that the equilibrium configuration of lipid and water molecules remained plausible at least up to 12 ns without SHAKE, as compared with not only earlier numerical results (11,13,14,23) but also experimental ones (30). For example, the average interfacial areas per lipid molecule were 67 Å^2 in the larger system and 64 Å^2 in the smaller one, and they are included in the range of experimental values from 56 Å^2 to 72 Å^2 reported in a review article (30). The obtained equilibrium bilayer/water system was utilized for the preparation of the initial configuration for the shock wave simulations.

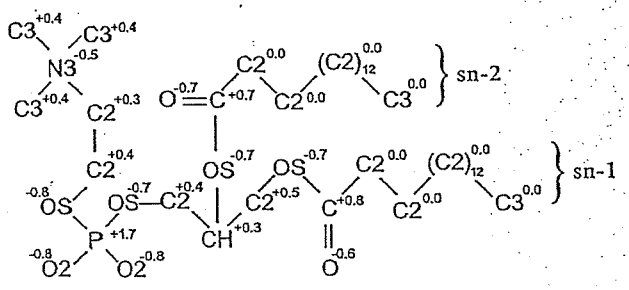

FIGURE 1 Atomic charges and AMBER atom types of DPPC molecule.

Modeling of shock waves

In the previous experiment (6), it was shown that the transport of fluorophores across the membranes of leukemia cells is governed by the shock impulse rather than the maximum pressure. The shock impulse per unit area I is defined as

$$I = \int_0^{t_+} p(t)dt, \tag{1}$$

where t is the time, $p(t)$ is the pressure near the cells in water, and t_+ is the positive phase duration of a half cycle of the shock wave (6). The experiment (6) was carried out with different types of shock waves produced by a laser and a shock tube. Their peak pressures and shock-pulse durations were considerably different, and therefore the shock impulse defined by Eq. 1 was introduced to examine the effect of shock waves on the cell permeabilization systematically.

From the definition of impulse, the shock impulse I can be regarded as the increment of momentum of water divided by an area A on which the pressure $p(t)$ is exerted. That is,

$$I = \frac{M(t_+) - M(0)}{A}, \tag{2}$$

where $M(t)$ is the momentum of water at time t. At time $t = 0$, the shock wave did not reach the cells and water ahead of the shock wave was at rest, and hence $M(0) = 0$. When $t = t_+$, the shock wave passed a small volume of water near the cells and the momentum $M(t_+) = I \times A$ was transferred to the small volume of water.

The shock waves in the experiment were pulses with duration times of at least 180 ns, corresponding to the pulse width of ~270 μm in water. It is impossible or prohibitively expensive to reproduce such shock waves in the simulation box with a periodic boundary condition. In this study, we numerically expressed the shock impulse by the momentum $M(t_+)$ of water molecules. More precisely, at the beginning of shock wave simulation, we added the momentum $M(t_+) = I \times A$ to water molecules in a volume $A \times L_Z$ adjacent to the bilayer, where the area A is the cross-sectional area normal to the z direction of the simulation box, e.g., $A = 7.18 \times 5.99$ nm $= 43.01$ nm^2 in the larger system, and L_Z is the length of the volume in the z direction (see Fig. 2). The choice of L_Z is arbitrary, and we put $L_Z = 4$ nm, which is almost equal to the initial thickness of bilayers, because this simulation was focused on the behavior of bilayers with the excess momentum $M(t_+)$ added by shock wave. The momentum change of water molecules at the beginning of shock simulation was numerically implemented by the addition of an average velocity V to the thermal velocity of water molecules in the equilibrated bilayer/water system, as shown in Fig. 2. The average velocity V is given by

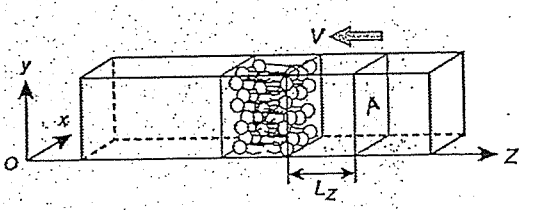

FIGURE 2 Schematic of the initial configuration of shock wave simulation. The average velocity V defined by Eq. 3 is added to water molecules in a volume $A \times L_Z$, where A is the cross-sectional area of simulation box, and $L_Z = 4$ nm. The *NVE* MD simulations were performed from this initial configuration.

$$V = \frac{M(t_+)}{mN} = \frac{I \times A}{mN}, \quad (3)$$

where m is the weight of a water molecule and N (almost 4000 in the larger system and almost 1000 in the smaller one) is the number of water molecules in the volume $A \times L_Z$. The impulse I was increased from 0 to 100 mPa·s at an interval of 2.5 mPa·s, and then V was changed from 0 to 25,600 m/s. Note that the impulse I used in the simulation was very small compared with that in the experiment (6), which was typically 100 Pa·s, although the average velocity V in the simulation appeared to be large. If the impulse I is raised to 100 Pa·s, the required average velocity V is 10^4 times larger than the sound speed in water. The average velocity V corresponds neither to the sound speed of liquid water nor to the propagation speed of the shock wave. It just represents the increase of momentum of water molecules due to the shock wave. The modeling of shock waves by the impulse makes the qualitative comparison possible between the numerical results in this work and the previous experimental ones.

Unsteady nonequilibrium simulation

We performed constant-volume MD simulation (*NVE* simulation) without using the control of temperature and pressure and the SHAKE algorithm from the initial configuration shown in Fig. 2. The periodic boundary conditions were applied in the three directions. The time step for integration of equations of motion was varied from $\tau = 2.0$ fs to 0.78 fs according to the size of V to avoid the excess approach of molecules with large velocities. The AMBER 7 set of programs (31) was used for computations.

Owing to the periodic boundary conditions, the simulations should be terminated at the time when the effect of the shock impulse reached the boundary at the opposite side of the simulation box. To simulate the essential part of structural changes of the bilayer before the termination of the simulation, sufficiently thick water regions were required in both sides of the bilayer in the simulation box. We therefore used the bilayer/water system with a large water layer of thickness ~14 nm.

ANALYSIS

The conspicuous structural change of bilayers in the dynamical process under the action of the shock impulse was the collapse and rebound of bilayers. In this study, the collapse and rebound of bilayers were analyzed by evaluating the thickness of bilayers, which was defined as the distance between phosphorous atoms in the headgroups of lipid molecules in upper and lower sides of bilayer. This definition is reasonable because two peaks in the electron density profile across the bilayer correspond to the locations of phosphorous atoms (23).

In the collapse and rebound stages of bilayers, the ordering in the tails (acyl chains) of lipid molecules was considerably different from that in the equilibrium state. The order parameter S_{CD} (11,14,32) is widely known to be a useful measure for the ordering of lipid molecules in equilibrium states, and usually S_{CD} is evaluated in a long-time average. In the analysis of collapsing and rebounding bilayers, the application of long-time averages should be bypassed, and therefore we used an averaged instantaneous order parameter $\hat{S}_{CD}$ defined as

$$\hat{S}_{CD} = -\frac{1}{2}\hat{S}_{zz} = -\frac{1}{2}\left(\frac{1}{N_C}\sum_{i=1}^{N_C}\frac{1}{2}(3\cos^2\Theta_i - 1)\right), \quad (4)$$

where Θ_i is the angle between the axis of the ith molecular axis and the bilayer normal (the z axis) and N_C (= 28) is the number of carbons in both *sn*-1 and *sn*-2 chains (see Fig. 1). The angle Θ_is were evaluated from the instantaneous configurations of lipid molecules. By definition, in the equilibrium states, $-\hat{S}_{CD}$ is equal to the average of the usual $-S_{CD}$ over all carbons in acyl chains, the value of which is estimated as ~0.16 from an earlier numerical result (11).

The fluidity of lipid molecules within the bilayer plane (the xy plane) has often been studied by means of the diffusion coefficient in the equilibrium MD simulations (33). However, the diffusion coefficient was not an appropriate measure of the fluidity in a high-speed phenomenon in the unsteady and nonequilibrium state. To quantify the lateral fluidity of lipids in the bilayer plane in unsteady states, we introduced an accumulated lateral displacement A_{LD} defined as

$$A_{LD}(t) = \sum_{k=0}^{n-1}\frac{1}{N_B}\sum_{i=1}^{N_B}|r_i((k+1)\Delta t) - r_i(k\Delta t)|, \quad (5)$$

where r_i is the distance from an origin of the xyz coordinates to the projection of the position of mass center of the ith lipid molecule onto the xy plane, N_B (= 32 or 128) is the number of lipid molecules in the bilayer, Δt (= 8τ) is a time interval for producing a configuration frame, k is the frame number, and $n = t/\Delta t$. Note that A_{LD} is independent of the choice of the origin of the coordinate system, and it increases with increase in the movement of lipid molecules in the bilayer.

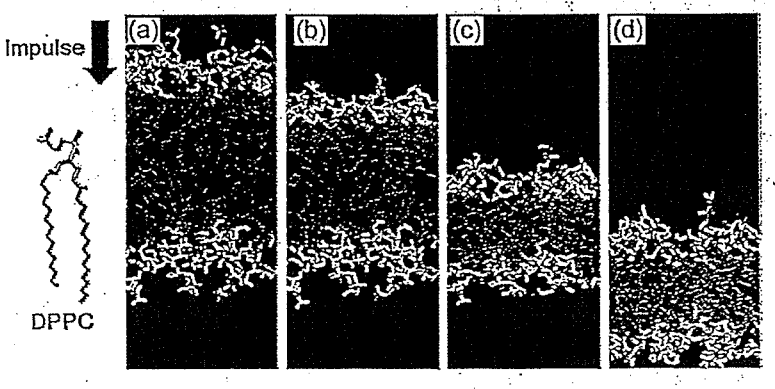

FIGURE 3 A series of snapshots of the collapse and rebound of lipid bilayer under the action of shock impulse of $I = 50$ mPa·s. The impulse was applied downwards. The headgroups of DPPC are shown in yellow and the acyl chains in green. Water molecules are not shown for clarity of presentation. (*a*) Equilibrium state; (*b*) 0.15 ps after the application of shock impulse. The upper layer began to move downwards; (*c*) 0.30 ps. The lower layer began to move; (*d*) 0.45 ps. The rebound stage of bilayer. The snapshots were made with the VMD program (Humphrey, W., Dalke, A., and Schulten, K. 1996. *J. Mol. Graph. Model.* 14:33–38).

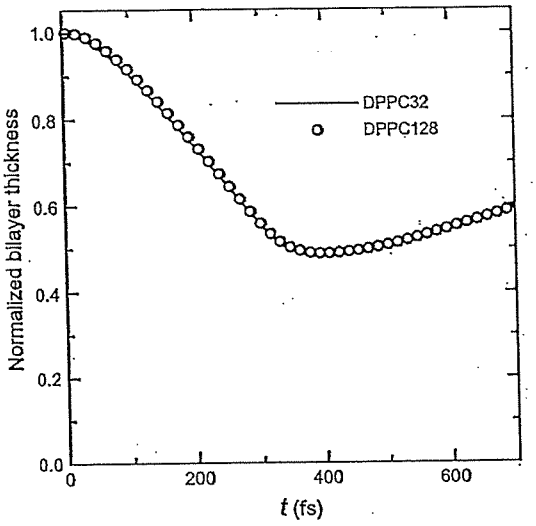

FIGURE 4 The evolution of bilayer thickness normalized by its initial value (4 nm) at $I = 50$ mPa·s. The solid curve represents the result with the smaller system (32 lipids) and the open circles that with the larger system (128 lipids).

We also examined the growth rate of A_{LD}, defined as dA_{LD}/dt, which should be a constant in an equilibrium state.

The transport of water molecules into the bilayer was the most important phenomenon in the results of these simulations. It has been suggested experimentally (34,35) and confirmed numerically (11,13) that very few water molecules exist beyond the carbonyl group in the *sn*-1 chain (see Fig. 1) in equilibrium states. Accordingly, when a water molecule entered a hydrophobic region between the carbonyl groups in *sn*-1 chains in upper and lower sides of bilayers in the simulation, we decided that the water molecule was transported into the bilayer.

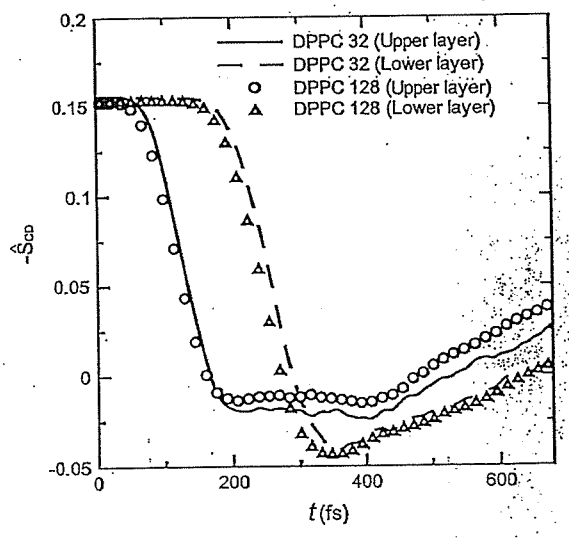

FIGURE 5 The temporal change of averaged instantaneous order parameter $\hat{S}_{CD}$ defined by Eq. 4 at $I = 50$ mPa·s.

RESULTS AND DISCUSSION

Collapse and rebound of bilayers

Fig. 3 is a series of snapshots in a typical result of shock wave simulation for $I = 50$ mPa·s and $V = 12{,}800$ m/s, where the collapse and rebound of bilayers are clearly shown. The excess momentum of shock impulse propagated downwards, first pushing down the upper layer and keeping the lower layer intact (see Fig. 3, *b* and *c*). Finally, the excess

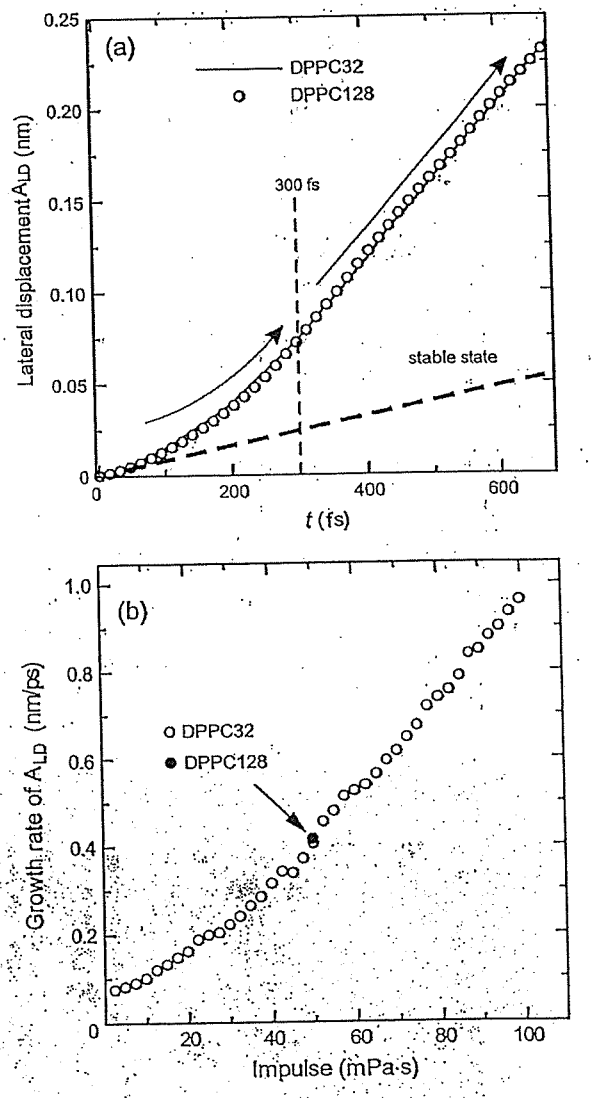

FIGURE 6 (*a*) Accumulated lateral displacement A_{LD} defined by Eq. 5 at $I = 50$ mPa·s. The behavior of A_{LD} is explained by the solid curves with arrows. (*b*) The change of the growth rate dA_{LD}/dt in the rebound stage for varying shock impulse.

momentum was transferred to the lower layer and it was also pushed down (Fig. 3 *d*). At that time, since the excess momentum had already passed the upper layer, the force pushing it down became weak, and the rebound stage set in. In this case, the simulation was terminated at $t = 700$ fs. The change of bilayer thickness is shown in Fig. 4. One can see that it decreased to almost half of the initial value (4 nm) at ~350 fs from the instant of shock impulse impact, and then it rebounded slowly. The numerical result in the smaller system completely agrees with that in the larger system.

The thickness of a bilayer is closely related to the length of acyl chains in the bilayer. The change of chain length can be characterized by the averaged instantaneous order parameter $\hat{S}_{CD}$, because the chain length becomes small if the disorder of chain bend angles increases. In Fig. 5, we present the temporal changes of $-\hat{S}_{CD}$s of the upper and lower layers separately for the case of $I = 50$ mPa·s. Before the beginning of collapse, both $-\hat{S}_{CD}$s were equal to 0.16 as expected from knowledge of the equilibrium state (11). As the shock impulse propagated downwards in the bilayer, first the $-\hat{S}_{CD}$ of the upper layer and then that of the lower layer began to decrease, and the time lag was ~0.1 ps, which corresponded to the time that the shock impulse passed the bilayer. The two $-\hat{S}_{CD}$s were rapidly reduced until reaching their minimum values, and the following rebound process was relatively slow. From the comparison with Fig. 4, it is immediately realized that the change of bilayer thickness was due to the change of chain bend angles.

Fluidity of lipid molecules

Fig. 6 *a* shows the temporal evolution of the accumulated lateral displacement A_{LD}, defined by Eq. 5, for the case of $I = 50$ mPa·s. In the stable state (equilibrium state), it constantly grows with time, as indicated by a bold broken line in the figure. On the other hand, the growth of A_{LD} in the shock wave simulation was composed of two stages: in the first stage from $t = 0$ to $t = 300$ fs, the growth rate dA_{LD}/dt gradually increased, and in the second stage after $t = 300$ fs, it was almost constant, as indicated by thin solid curves with arrows. These two stages precisely agreed with the collapse and rebound stages of bilayers shown in Figs. 3–5. In particular, it is worth noting that the growth rate was hardly weakened in the rebound stage.

Fig. 6 *b* shows that the growth rate dA_{LD}/dt in the second stage was an increasing function of shock impulse. In the equilibrium state it is not 0 but ~0.1 nm/ps (see Fig. 6 *a*). However, despite the nonzero growth rate, very few water molecules enter the hydrophobic region in the equilibrium state, as mentioned before. Therefore, the continuance of high fluidity, i.e., the large growth rate for some period, seems to play an essential role for the penetration of water molecules because the growth rate can be regarded as a measure of the lateral fluidity of lipid molecules.

Water penetration into the hydrophobic region

The application of shock impulse to bilayer induced the penetration of water molecules in the hydrophobic region of the bilayer. In the following, we demonstrate how the water molecules penetrated into the bilayer and discuss this important phenomenon.

Fig. 7 is a series of snapshots for the same result as that shown in Fig. 3 (in a slight close-up). In the figure, acyl chains are eliminated and water molecules are indicated by blue spots. The penetration of water molecules into the hydrophobic region of the bilayer is shown clearly. Note that, as can be seen from Fig. 7 *a*, even in the equilibrium state (before the arrival of the shock impulse), several water molecules exist near the lipid headgroups shown in yellow. However, they are outside the hydrophobic region between the carbonyl groups in *sn*-1 chains in upper and lower sides of the bilayer, and they cannot enter the hydrophobic region without the action of the shock impulse in the timescale of MD simulations.

We plot the number of water molecules in the hydrophobic region in Fig. 8 *a* for the case of $I = 50$ mPa·s. Except for

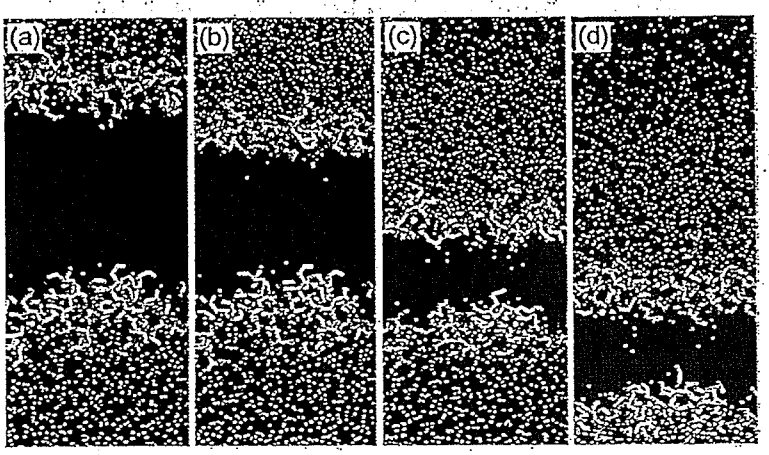

FIGURE 7 A series of snapshots of water penetration for the same result as that shown in Fig. 3. Water molecules are signified by blue spots, and acyl chains are eliminated. (*a*) Equilibrium state; (*b*) 0.15 ps. Some water molecules were carried into the hydrophobic region; (*c*) 0.30 ps; (d) 0.45 ps. Even in the rebound stage, water molecules still penetrated into the hydrophobic region.

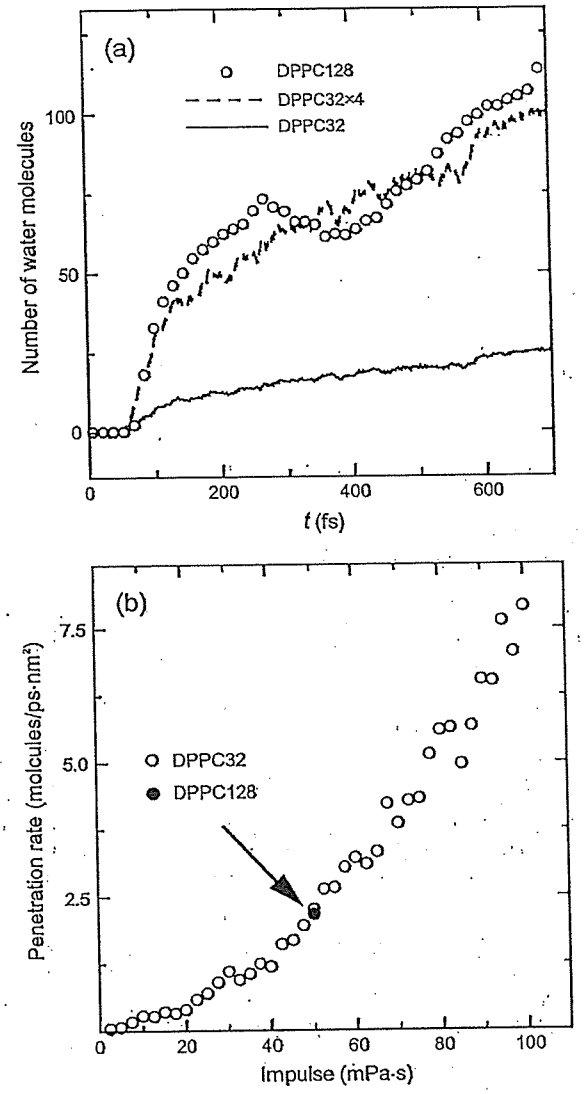

FIGURE 8 (*a*) The number of water molecules in the hydrophobic region at $I = 50$ mPa·s. The broken line denotes the penetration rate except for the beginning of collapse of bilayer. (*b*) The penetration rate of water molecules versus shock impulse.

the beginning of the collapse stage, the number of water molecules increased with time at a constant rate (100 molecules/ps) even after the rebound stage began (300 fs). This means that the rebound stage is more significant for water penetration than the collapse stage, although the structural change (bilayer shrinkage and acyl chain disorder) occurs much more violently in the collapse stage. The number of water molecules in the hydrophobic region in the larger system of 128 lipids is four times as large as that in the smaller system of 32 lipids, as expected.

In Fig. 8 *b*, we illustrate how the number of penetrated water molecules increased with the increase in shock impulse. The ordinate in the figure represents the number of water molecules in the hydrophobic region at the instant of termination of simulation divided by the cross-sectional area ($A = 43.01$ nm^2 in the larger system and 10.25 nm^2 in the smaller one) and the simulation time. The rate of water penetration in the rebound stage can be estimated as ~2.5 molecules/ps·nm^2 in the case of $I = 50$ mPa·s and it exceeded 7.5 molecules/ps·nm^2 in the case of $I = 100$ mPa·s. We remark that the trend observed in Fig. 8 *b* is similar to that of the growth rate of A_{LD} shown in Fig. 6 *b*. That is, as the shock impulse increases, the lateral fluidity of lipid molecules increased and so did the number of penetrated water molecules.

As shown in Fig. 8 *b*, the number of penetrated water molecules increased with increasing shock impulse. This qualitatively agrees with the previous experiment (6), although there were a few differences: in the experiment, calcein (622 Da) and fluorescein isothiocyanate dextran (71.6 kDa) were delivered into the cells by the shock impulse of 100 Pa·s, whereas in the simulation, water (18 Da) penetrated into the bilayer by the impulse of at most 100 mPa·s. This may be a reflection of the fact that the transport of large molecules across cell membranes requires a large amount of impulse.

The mass density profile of water molecules in the case of $I = 50$ mPa·s is illustrated in Fig. 9, where Fig. 9 *a* shows the initial profile and the shading indicates the hydrophobic region. From the figure, it is clear that water molecules are carried into the hydrophobic region (see Fig. 7) and the shrinkage and recovery of the hydrophobic region are

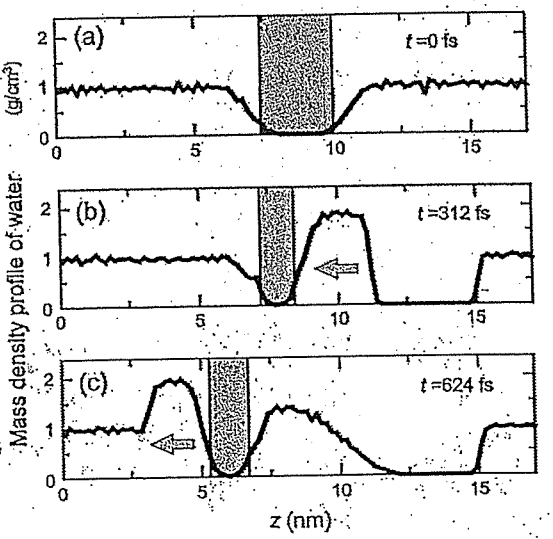

FIGURE 9 The mass density profiles for the case of $I = 50$ mPa·s in the larger system of 128 lipids. The mass density is evaluated by counting the number of water molecules in a slab of width 1.74 Å. The direction of propagation of shock wave is indicated by arrows. (*a*) The initial profile. (*b*) At $t = 312$ fs, a high density water region appears near the bilayer and water molecules have already been transported into the hydrophobic region indicated by the shading. (*c*) At $t = 628$ fs, a high density water region appears in the opposite side of the bilayer.

induced by high density water. An empty region behind the high density water (12 nm $< z <$ 15 nm) is caused by the velocity difference in the initial condition.

These shock wave simulations were limited to a relatively small bilayer/water system. Nevertheless, as a result of careful simulations and analyses, we clarified several important features in the dynamical process of lipid bilayers under the action of shock impulses, which had never been investigated, to our knowledge, from the molecular point of view. Now, on the basis of these numerical results, we propose a possible mechanism of molecular transport of external macromolecules across the cell membrane by the shock wave. Unlike the penetration of water molecules, the transport of macromolecules requires a transient pore filled with water in the cell membrane, as several authors have considered (5,19–22). As shown in these simulations, the action of the shock impulse results in the penetration of water molecules and is not directly connected to the pore formation. We predict that the inclusion of a large number of water molecules in the hydrophobic region of the bilayer leads to the spontaneous pore formation in the cell membrane after the shock wave has gone. This will be demonstrated in a forthcoming work.

SUMMARY

Unsteady and nonequilibrium MD simulations of the interaction of a single shock impulse with a lipid bilayer were performed. The detailed picture of the structural change in the bilayer was clarified to be composed of the two stages, the collapse and rebound stages. The change of the bilayer thickness, the distribution of chain bend angles, the lateral fluidity of lipid molecules, and the subsequent water penetration into the hydrophobic region were examined. These structural changes depended on the intensity of the shock impulse, and the results showed the qualitative agreement with those in the previous experiment. We found that the lateral fluidity of lipid molecules continued to be large for some period in the rebound stage without being weakened, and it is in this rebound stage that water molecules are transported into the hydrophobic region of the bilayer at a constant rate for a given shock impulse.

T.K. was supported by grants from Special Coordination Funds for Promoting Science and Technology (MEXT), Grant-in-Aid for Scientific Research on Priority Areas, MEXT (17012002, 18014002), Grant-in-Aid for Exploratory Research, JSPS (18650140), Grant-in-Aid for Scientific Research (B), JSPS (17300168), and Research on Advanced Medical Technology, Health Labor Sciences Research Grant, the Ministry of Health, Welfare and Labor, Japan (H17-nano-006).

REFERENCES

1. Gambihler, S., and M. Delius. 1992. Transient increase in membrane permeability of L1210 cells upon exposure to lithotripter shock waves in vitro. *Naturwissenschaften.* 79:328–329.
2. Doukas, A. G., D. J. McAuliffe, and T. J. Flotte. 1993. Biological effects of laser-induced shock waves: structural and functional cell damage in vitro. *Ultrasound Med. Biol.* 19:137–146.
3. Gambihler, S., M. Delius, and J. W. Ellwart. 1994. Permeabilization of the plasma membrane of L1210 mouse leukemia cells using lithotripter shock waves. *J. Membr. Biol.* 141:267–275.
4. Delius, A., and G. Adams. 1999. Shock wave permeabilization with ribosome inactivating proteins: a new approach to tumor therapy. *Cancer Res.* 59:5227–5232.
5. Rosenthal, I., J. Z. Sostaric, and P. Riesz. 2004. Sonodynamic therapy—a review of the synergistic effects of drugs and ultrasound. *Ultrason. Sonochem.* 11:349–363.
6. Kodama, T., M. R. Hamblin, and A. G. Doukas. 2000. Cytoplasmic molecular delivery with shock waves: importance of impulse. *Biophys. J.* 79:1821–1832.
7. Kodama, T., A. G. Doukas, and M. R. Hamblin. 2002. Shock wave-mediated molecular delivery into cells. *Biochim. Biophys. Acta.* 1542:186–194.
8. Singer, S. J., and G. L. Nicholson. 1972. The fluid mosaic model of the structure of cell membranes. *Science.* 175:720–731.
9. Simons, K., and E. Ikonen. 1997. Functional rafts in cell membranes. *Nature.* 387:569–572.
10. Edidin, M. 2003. The state of lipid rafts: from model membranes to cells. *Annu. Rev. Biophys. Biomol. Struct.* 32:257–283.
11. Berger, O., O. Edholm, and F. Jahnig. 1997. Molecular dynamics simulations of a fluid bilayer of dipalmitoylphosphatidylcholine at full hydration, constant pressure, and constant temperature. *Biophys. J.* 72:2002–2013.
12. Chiu, S. W., M. Clark, V. Balaji, S. Subramaniam, H. L. Scott, and E. Jakobsson. 1995. Incorporation of surface tension into molecular dynamics simulation of an interface: a fluid phase lipid bilayer membrane. *Biophys. J.* 69:1230–1245.
13. Shinoda, W., N. Namiki, and S. Okazaki. 1997. Molecular dynamics study of a lipid bilayer: convergence, structure, and long-time dynamics. *J. Chem. Phys.* 106:5731–5743.
14. Patra, M., M. Karttunen, M. T. Hyvonen, E. Falck, P. Lindqvist, and I. Vattulainen. 2003. Molecular dynamics simulations of lipid bilayers: major artifacts due to truncating electrostatic interactions. *Biophys. J.* 84:3636–3645.
15. Tieleman, D. P., and J. Bentz. 2002. Molecular dynamics simulation of the evolution of hydrophobic defects in one monolayer of a phosphatidylcholine bilayer: relevance for membrane fusion mechanisms. *Biophys. J.* 83:1501–1510.
16. Zhu, F., E. Tajkhorshid, and K. Schulten. 2002. Pressure-induced water transport in membrane channels studied by molecular dynamics. *Biophys. J.* 83:154–160.
17. Ulander, J., and A. D. J. Haymet. 2003. Permeation across hydrated DPPC lipid bilayers: simulation of the titrable amphiphilic drug valproic acid. *Biophys. J.* 85:3475–3484.
18. Bemporad, D., C. Luttmann, and J. W. Essex. 2004. Computer simulation of small molecule permeation across a lipid bilayer: dependence on bilayer properties and solute volume, size, and cross-sectional area. *Biophys. J.* 87:1–13.
19. Tieleman, D. P. 2004. The molecular basis of electroporation. *BMC Biochem.* 5:10:1–12.
20. Leontiadou, H., A. E. Mark, and S.-J. Marrink. 2004. Molecular dynamics simulations of hydrophilic pores in lipid bilayers. *Biophys. J.* 86:2156–2164.
21. Tarek, M. 2005. Membrane electroporation: a molecular dynamics simulation. *Biophys. J.* 88:4045–4053.
22. Gurtovenko, A. A., and I. Vattulainen. 2005. Pore formation coupled to ion transport through lipid membranes as induced by transmembrane ionic charge imbalance: atomistic molecular dynamics study. *J. Am. Chem. Soc.* 127:17570–17571.
23. Smondyrev, A. M., and M. L. Berkowitz. 1999. United atom force field for phospholipid membranes: constant pressure molecular dynamics simulation of dipalmitoylphosphatidicholine/water system. *J. Comput. Chem.* 20:531–545.

24. Wang, J. M., P. Cieplak, and P. A. Kollman. 2000. How well does a restrained electrostatic potential (RESP) model perform in calculating conformational energies of organic and biological molecules? *J. Comput. Chem.* 21:1049–1074.

25. Berendsen, H. J. C., J. P. M. Postma, W. F. van Gunsteren, and J. Hermans. 1981. Interaction models for water in relation to protein hydration. *In* Intermolecular Forces. B. Pullman, editor. Reidel Publishing Company, Dordrecht, The Netherlands. 331–342.

26. Essmann, U., L. Perera, M. L. Berkowitz, T. Darden, H. Lee, and L. G. Pedersen. 1995. A smooth particle mesh Ewald method. *J. Chem. Phys.* 103:8577–8593.

27. Berendsen, H. J. C., J. P. M. Postma, W. F. van Gunsteren, A. DiNola, and J. R. Haak. 1984. Molecular dynamics with coupling to an external bath. *J. Chem. Phys.* 81:3684–3690.

28. Ryckaert, J. P., G. Ciccotti, and H. J. C. Berendsen. 1977. Numerical integration of the Cartesian equations of motion of a system with constraints: molecular dynamics of *n*-alkanes. *J. Comput. Phys.* 23:327–341.

29. Marrink, S.-J., O. Berger, P. Tieleman, and F. Jähnig. 1998. Adhesion forces of lipids in a phospholipid membrane studied by molecular dynamics simulations. *Biophys. J.* 74:931–943.

30. Nagle, J. F., and S. Tristram-Nagle. 2000. Structure of lipid bilayers. *Biochim. Biophys. Acta.* 1469:159–195.

31. Pearlman, D. A., D. A. Case, J. W. Caldwell, W. S. Ross, T. E. Cheatham, S. Debolt, D. Ferguson, G. Siebel, and P. Kollman. 1995. AMBER, a package of computer-programs for applying molecular mechanics, normal-mode analysis, molecular dynamics and free-energy calculations to simulate the structural and energetic properties of molecules. *Comput. Phys. Commun.* 91:1–41.

32. Egberts, E., and H. J. C. Berendsen. 1988. Molecular dynamics simulation of a smectic liquid crystal with atomic detail. *J. Chem. Phys.* 89:3718–3732.

33. Almeida, P. F. F., and W. L. C. Vaz. 1995. Lateral diffusion in membranes. *In* Handbook of Biological Physics, Vol. 1. Structure and Dynamics of Membrane. R. Lipowsky and E. Sackmann, editors. Elsevier, Amsterdam. 305–357.

34. Zaccai, G., J. K. Blasie, and B. P. Schoenborn. 1975. Neutron diffraction studies on the location of water in lecithin bilayer model membranes. *Proc. Natl. Acad. Sci. USA.* 72:376–380.

35. Büldt, G., H. U. Gally, and J. Seelig. 1979. Neutron diffraction studies on phosphatidylcholine model membranes. *J. Mol. Biol.* 134:673–691.

IV

EMERGING TECHNOLOGIES USING ULTRASOUND FOR DRUG DELIVERY

Katsuro Tachibana and Shunro Tachibana

Therapeutic ultrasound has mainly been applied for its thermal or mechanical effects. Medical applications of high-energy ultrasound to ablate cancers are now under investigation. Recently, there have been numerous reports on the application of non-thermal ultrasound energy for treating various diseases in combination with drugs. Furthermore, the introduction of microbubbles and nanobubbles as carriers/enhancers of drugs has added a whole new dimension to therapeutic ultrasound. Progress in the past decade from the pharmaceutical side has further added much excitement in applying this technology especially in the field of molecular biology, gene therapy and regenerative medicine. Alternatively, from the device side, therapeutic ultrasound catheters and extracorporeal ultrasound probes are under development specifically for this purpose, with some already in clinical trials. Examples such as enhancement of thrombolytic agents by ultrasound have proven to be beneficial for patients with acute strokes and peripheral arterial occlusions. Non-invasive focused ultrasound in conjunction with anti cancer drugs may help to reduce tumor size and lessen recurrence, as well as reduce severe drug side effects. Chemical activation of drugs by ultrasound energy for the treatment of atherosclerosis and tumors is another new field recently termed as "Sonodynamic Therapy". Lastly, advances in molecular imaging have also initiated great expectations in applying ultrasound for both diagnosis and therapy at the same time. Microbubbles or nanobubbles targeted at the molecular level will permit medical doctors to make a final diagnosis of a disease by ultrasound and immediately proceed

to therapeutic ultrasound. This chapter will put emphasis on emerging technologies in therapeutic ultrasound related to the above topics.

1. Introduction

A completely new concept of using non-thermal ultrasound in conjunction with drug has broadened the scope of therapeutic ultrasound. Characterized ultrasound thermal bioeffects and their application have been studied previously, but relatively few researchers have investigated the possibility of using nonthermal ultrasound as a means to enhance the effectivity of drugs until recently. Non-thermal mechanisms include various forms of energy such as cavitation, acoustic streaming, micro jets and radiation force which increases possibilities for targeting tissue with drugs and enhancing drug effectiveness or even chemically activating certain materials. In these applications, the ultrasound itself produces only minimal damage to tissues; the bioeffects that occur lead to a beneficial outcome for drug therapy.

In order to discuss the significance of ultrasound application in conjunction with drugs, one must understand the pharmacological background involved. Although there are thousands of types of drugs available for use today, the number of drugs that never reached the market may be ten-fold or even a hundred-fold greater. These types of drugs either had severe side effects or proven to be ineffective during the preclinical or early clinical trials. The various agents for cancer chemotherapy are of these types. Some of these agents administered systemically can kill solid tumors, but severely damage healthy tissues and organs at the same time too. Renal or heart failure and liver dysfunction are not rare among cancer patients treated with these highly toxic chemotherapeutic agents. A tumor site-specific drug is definitely needed in this case. On the other hand, drugs for hypertension require a 24-hour elevated drug concentration level in order to maintain stable blood pressure. As still another requirement, intermittent insulin injection is needed after each meal for diabetic patients. A new drug release system which could eliminate frequent oral administration of the drug is desired. These issues have been a major limitation and a challenge to pharmacologists for many years. Pharmaceutical companies have attempted to address these problems by suggesting the concept or strategy termed "drug delivery system (DDS)" since the 70s. The two keywords for DDS are

"targeting" and "controlled release". The major goal was to avoid severe side effects by reducing the total dosage, but at the same time concentrating the drug at the target site. Additionally, controlled drug release permits more control over the amount of drug administered in a certain time frame. Recent progress in the application of ultrasound energy for DDS has demonstrated it to be a promising modality for both "targeting" and "controlled release" of drugs.

The application of nonthermal ultrasound for DDS can be classified into three major categories. Firstly, ultrasound energy can actually help agents penetrate through various tissues. It has been demonstrated that acoustic pressure can "push" materials into the skin (please see Chap. VII), blood clots or other tissues. Secondly, ultrasound can have a direct effect on the membrane and change the permeability or absorption of the drug into cells (please see Chap. VI) and tissues. Lastly, ultrasound can "release" drugs from a certain drug carrier or change the chemical properties of the drug itself at localized site (Fig. 1). For a general discussion of mechanisms for

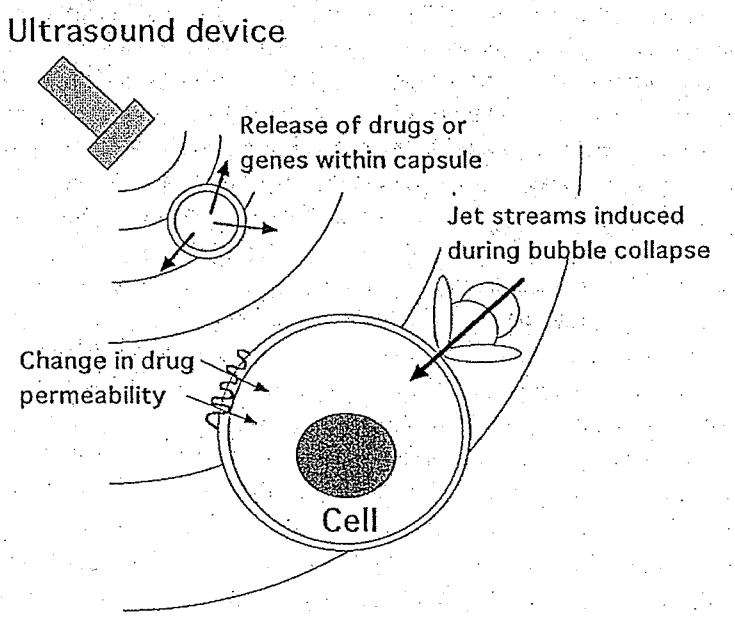

Fig. 1. Major mechanism believed to be involved in drug delivery by ultrasound.

biological effects of ultrasound, please refer to Chap. II. Microbubbles and nanobubbles can carry and release a certain drug at a specific target site and a particular time by ultrasound. Ultrasound-sensitive materials such as hematoporphyrin, a nontoxic agent, can also be activated by ultrasound at a localized lesion and can thus result in killing cancer cells. A wide variety of applications for drug delivery with ultrasound are currently under investigation in many fields. The most futuristic investigation under progress is the use of ultrasound for gene therapy (please see Chap. III). The DNA can be injected through the cell membrane as if a "micro syringe" were used and induce transfection with ultrasound energy. Induction of gene transfer by ultrasound to the cell could result in regeneration of blood vessels, nerves or any other tissue. With the help of microbubbles or nanobubbles, it is possible to change the permeability of drugs in the microscopic cell membrane level. Recent experimental data using ultrasound for gene therapy suggests that this technology could prove to be critical for some of the emerging "next generation" drugs in the clinical context.

2. Historical Background

Although the potential of ultrasound, with nonthermal mechanism, as a means to deliver various drugs has achieved its status as of this date, with many papers appearing from around the world to support it, the ultrasound medical society and industry were initially very slow in responding, and at times coldly rejecting the concept itself. In retrospect, ultrasound imaging researchers and the industry in the 80s and 90s may or may not have intentionally defined thermal ultrasound as the main or only cause of bioeffects and applicable for therapy. This resulted in the misperception that non-thermal ultrasound was for imaging alone and should be completely harmless and safe without induction of bioeffects. Another obstacle that hampered recognition of this technology was the lack of knowledge on the pharmaceutical side, where nothing was known about devices such as those that are used in medical ultrasound. *Vice versa*, the device side knew nothing about drugs. Finally, multidisciplinary research programs were needed to understand the mechanism of the interaction between drugs and ultrasound, as well as the final biological outcome. These types of research was not frequent in those days. Investigational research on ultrasound-drug relationships was not an easy task for both acoustic physicists or biologists.

The complexity of the technology also prevented venture companies and investment from developing products, fearing lengthy approval rounds with the FDA. Within the FDA, the approval process was completely separate between the medical device and the pharmaceutical division which prevented rapid penetration of this technology into the medical market. The rare exception of FDA approval of a device-drug combination therapy product occurred in the early 90s. This product was the combination of a photosensitive drug and lasers that chemically activate it for early lung and gastric cancer (photodynamic therapy, PDT). Meanwhile, a handful of diligent scientists continued to produce ultrasound/drug related papers over the years and finally brought the technology to its broader scope today.

In 1976, Kremkau *et al.* were the first to study the cytotoxic effects of various anti cancer drugs, such as nitrogen mustard, to mouse leukemia L1210 in combination with ultrasound irradiation. Although ultrasound energy clearly enhanced the cytotoxicity of drugs, it was not determined if this enhancement was due to ultrasound or hyperthermic effect on the cells. It was later discovered from the experiments that the increase in drug efficiency cannot be completely explained by mere temperature elevation induced by ultrasound treatment. A nonthermal effect of ultrasound that interacts with drugs was suggested to be the mechanism involved. Saad *et al.* (1989) demonstrated, in a temperature-controlled experimental system, that synergistic cytotoxicity can be obtained by anti cancer drugs and ultrasound that was unrelated to hyperthermia. Experiments performed by Harrison *et al.* (1991) using low-intensity ultrasound without any temperature increase showed similar results. It was pointed out that low-level ultrasound may have altered the cell membrane, thus changing its permeability to the drug. Marked enhancement by ultrasound of the cytotoxicity of adriamycin and amphotericin B against Chinese hamster ovary cells HA1 at lower energies has been demonstrated by Harrison.

Tachibana *et al.* (1981) and Furuhata *et al.* (1989) discovered in the early 80s that the time needed to dissolve blood clots by lytic agents was significantly reduced when clots were irradiated with low intensity, nonthermal ultrasound. This finding led to much excitement in the treatment for acute myocardial and brain infarction, because shortening the duration of blood vessel occlusion by clots is a critical factor for better prognosis. Figure 2 shows the classical test tube experiment with the artificial fibrin